Spatiotemporal dynamics in optical energy transfer on the nanoscale and its application to constraint satisfaction problems

Makoto Naruse,[1,2,*] Masashi Aono,[3] Song-Ju Kim,[3] Tadashi Kawazoe,[2,5] Wataru Nomura,[2,5] Hirokazu Hori,[4] Masahiko Hara,[3] and Motoichi Ohtsu[2,5]

[1]*Photonic Network Research Institute, National Institute of Information and Communications Technology, 4-2-1 Nukui-kita, Koganei, Tokyo 184-8795, Japan*

[2]*Nanophotonics Research Center, Graduate School of Engineering, The University of Tokyo, 2-11-16 Yayoi, Bunkyo-ku, Tokyo 113-8656, Japan*

[3]*Flucto-order Functions Research Team, RIKEN Advanced Science Institute, 2-1, Hirosawa, Wako, Saitama 351-0198, Japan*

[4]*Interdisciplinary Graduate School of Medicine and Engineering, University of Yamanashi, Takeda 4-3-11, Kofu, Yamanashi 400-8511, Japan*

[5]*Department of Electrical Engineering and Information Systems Graduate School of Engineering, The University of Tokyo, 2-11-16 Yayoi, Bunkyo-ku, Tokyo 113-8656, Japan*

(Received 22 May 2012; revised manuscript received 10 July 2012; published 5 September 2012)

Nature-inspired devices and architectures are attracting considerable attention for various purposes, including developing novel computing based on spatiotemporal dynamics, exploiting stochastic processes for computing, and reducing energy dissipation. This paper demonstrates that the optical energy transfer between quantum nanostructures mediated by optical near-field interactions occurring at scales far below the wavelength of light could be utilized for solving constraint satisfaction problems (CSPs). The optical energy transfer from smaller quantum dots to larger ones, which is a quantum stochastic process, depends on the existence of resonant energy levels between the quantum dots or a state-filling effect occurring at the larger quantum dots. Such a spatiotemporal mechanism yields different evolutions of energy transfer patterns in multi-quantum-dot systems. We numerically demonstrate that optical energy transfer processes can be used to solve a CSP. The work described in this paper is a first step in showing the applicability and potential of nanometer-scale optical near-field processes toward solving computationally demanding problems.

DOI: 10.1103/PhysRevB.86.125407 PACS number(s): 78.67.−n, 05.10.−a, 05.30.−d

I. INTRODUCTION

There is great demand for novel computing devices and architectures that can overcome the limitations of conventional technologies based solely on electron transfer, in terms of reducing power dissipation, solving computationally demanding problems, and so on.[1] Also, nature-inspired architectures are attracting significant attention from various research arenas, such as brainlike computing and computational neurosciences,[2] stochastic-based computing and noise-based logic,[3] and spatiotemporal computation dynamics.[4]

Among these research topics, Nakagaki *et al*. showed that a single-celled amoebalike organism, a plasmodium of the true slime mold *Physarum polycephalum,* is capable of finding the minimum-length solutions between two food sources.[5] Also, Aono *et al*. demonstrated "amoeba-based computing," such as solving a constraint satisfaction problem (CSP) (Ref. 4) and the traveling salesman problem (TSP),[6] by utilizing the spatiotemporal oscillatory dynamics of the photoresponsive amoeboid organism *Physarum* combined with external optical feedback control. Aside from such experimental demonstrations, Leibtnitz *et al*. showed an algorithm for selecting the most suitable and robust network by utilizing fluctuations inspired by biological experiments where the speed of fluorescence evolution of proteins in bacteria is observed to have a positive correlation with the phenotypic fluctuation of fluorescence over clone bacteria.[7]

These demonstrations indicate that we can utilize the inherent spatial and temporal dynamics appearing in physical processes in nature for novel computing architectures and applications. Such arguments should also be applicable to nanometer-scale light-matter interactions. In fact, Naruse *et al*. demonstrated nanophotonic computing based on optical near-field processes at scales below the wavelength of light.[8] In particular, energy transfer between quantum nanostructures mediated by optical near-field interactions, detailed in Sec. II, plays a crucial role. Optical near-field interactions, which are described by a Yukawa-type potential, have realized energy transfer that involves conventionally dipole-forbidden energy levels. Its theoretical foundation has been explained by the dressed photon model,[9] and the process has been experimentally demonstrated in various quantum nanostructures such as InGaAs,[10] ZnO,[11] CdSe,[12] etc. In particular, Kawazoe *et al*. recently demonstrated room-temperature optical energy transfer using two-layer InGaAs quantum dots (QDs).[13] In addition, the optical energy transfer has been shown to be 10^4 times more energy efficient than that of the bit-flip energy required in conventional electrically wired devices.[14]

This article theoretically demonstrates that optical energy transfer between quantum dots mediated by optical near-field interactions can be utilized for solving a CSP. The optical energy transfer from smaller quantum dots to larger ones depends on the existence of resonant energy levels between the quantum dots or a state-filling effect occurring at the destination quantum dots. Also, as indicated by the quantum master equations, the energy transfer process is fundamentally probabilistic. Such a spatiotemporal mechanism yields different evolutions of energy transfer patterns combined with certain feedback mechanisms, similarly to the evolution of the shape of *Physarum* demonstrated by Aono *et al*. in

Ref. 4. At the same time, in contrast to biological organisms, optical energy transfer is implemented by highly controlled engineering means for designated structures, such as semiconductor quantum nanostructures based on, for instance, molecular beam epitaxy[15] or DNA-based self-assembly.[16] The operating speed of such optical-near-field–mediated quantum-dot systems, which is on the order of nanoseconds when radiative relaxation processes are involved, is significantly faster than those based on biological organisms, which is on the order of seconds or minutes.[4,6] The energy efficiency,[14] as indicated already above, and the possibility of room-temperature operation[13] are also strong motivations behind the investigations described in this paper. Other interesting nanomaterials, such as nanodiamonds,[17,18] could be considered in the implementation aside from semiconductor quantum dots. In addition, we should emphasize that the concept and the principles discussed in this paper are fundamentally different from those of conventional optical computing or optical signal processing, which are limited by the properties of propagating light.[19] The concept and principles are also different from the quantum computing paradigm where a superposition of all possible states is exploited so as to lead to a correct solution.[20] The optical-near-field–mediated energy transfer is a coherent process, suggesting that an optical excitation could be transferred to all possible destination QDs via a resonant energy level, but such coherent interaction between QDs results in a unidirectional energy transfer by an energy dissipation process occurring in the larger dot, as described in Sec. II. Thus, our approach opens up the possibility of another computing paradigm where both coherent and dissipative processes are exploited.

This paper is organized as follows. Section II characterizes state-dependent optical energy transfer via optical near-field interactions. Section III formulates the satisfiability problem studied in this paper, followed by an example demonstration. Section IV concludes the paper.

II. STATE-DEPENDENT OPTICAL ENERGY TRANSFER VIA OPTICAL NEAR-FIELD INTERACTIONS FOR SOLVING A CONSTRAINT SATISFACTION PROBLEM (CSP)

A. Energy transfer between quantum dots mediated by optical near-field interactions

First, we briefly review the fundamental principles of optical energy transfer involving optical near-field interactions.[9,21] We begin with the interaction Hamiltonian between an electron-hole pair and an electric field, which is given by

$$\hat{H}_{\rm int} = -\int d^3r \sum_{i,j=e,h} \hat{\psi}_i^{\dagger}(\mathbf{r}) e\mathbf{r}\cdot\mathbf{E}(\mathbf{r})\hat{\psi}_j(\mathbf{r}), \qquad (1)$$

where e represents the electron charge, $\hat{\psi}_i^{\dagger}(\mathbf{r})$ and $\hat{\psi}_j(\mathbf{r})$ are, respectively, creation and annihilation operators of either an electron ($i,j=e$) or a hole ($i,j=h$) at position $\mathbf{r}$, and $\mathbf{E}(\mathbf{r})$ is the electric field.[22] In usual light-matter interactions, $\mathbf{E}(\mathbf{r})$ is a constant since the electric field of diffraction-limited propagating light is homogeneous on the nanometer scale. Therefore, we can derive optical selection rules by calculating the dipole transition matrix elements. As a consequence, in the case of spherical quantum dots, for instance, only transitions to states specified by $l=m=0$ are allowed, where l and m are the orbital angular momentum quantum number and magnetic quantum number, respectively. In the case of optical near-field interactions, on the other hand, due to the large spatial inhomogeneity of the localized optical near fields at the surface of nanoscale material, an optical transition that violates conventional optical selection rules is allowed. Detailed theory and experimental details can be found in Ref. 23.

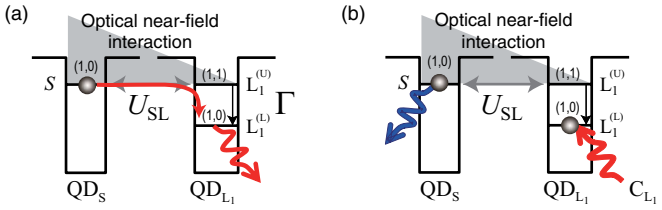

FIG. 1. (Color online) (a) Optical energy transfer between quantum dots mediated by optical near-field interactions. (b) State filling induced at the lower energy level in the larger dot by control light.

Here, we assume two spherical quantum dots whose radii are $R_{\rm S}$ and $R_{\rm L}$, which we call $\mathrm{QD_S}$ and $\mathrm{QD_{L_1}}$, respectively, as shown in Fig. 1(a). The energy eigenvalues of states specified by quantum numbers (n,l) are given by

$$E_{nl} = E_g + E_{ex} + \frac{\hbar^2\alpha_{nl}^2}{2MR^2} \quad (n=1,2,3,\ldots), \qquad (2)$$

where E_g is the band-gap energy of the bulk semiconductor, E_{ex} is the exciton binding energy in the bulk system, M is the effective mass of the exciton, and α_{nl} are determined from the boundary conditions, for example, as $\alpha_{n0}=n\pi$, $\alpha_{11}=4.49$. According to Eq. (2), there exists a resonance between the level with quantum number (1,0) in $\mathrm{QD_S}$, denoted by S in Fig. 1(a), and that with quantum number (1,1) in $\mathrm{QD_{L_1}}$, denoted by $\mathrm{L_1^{(U)}}$, if $R_{\rm L}/R_{\rm S}=4.49/\pi\approx 1.43$. Note that the (1,1) level in $\mathrm{QD_{L_1}}$ is a dipole-forbidden energy level. However, optical near fields allow this level to be populated by excitation.[23] Therefore, an exciton in the (1,0) level in $\mathrm{QD_S}$ could be transferred to the (1,1) level in $\mathrm{QD_{L_1}}$. In $\mathrm{QD_{L_1}}$, due to the sublevel energy relaxation with a relaxation constant Γ, which is faster than the near-field interaction, the exciton relaxes to the (1,0) level, denoted by $\mathrm{L_1^{(L)}}$, from where it radiatively decays. Also, because the radiation lifetime of quantum dots is inversely proportional to their volume,[24] finally we find unidirectional optical excitation transfer from $\mathrm{QD_S}$ to $\mathrm{QD_{L_1}}$.

In the optical excitation transfer discussed above, the energy dissipation occurring in the destination quantum dot determines the unidirectionality of energy transfer. Therefore, when the lower energy level of the destination quantum dot is filled with another excitation (called "state filling"), an optical excitation occurring in a smaller QD can not move to a larger one. As a result, the optical excitation will go back and forth between these dots (optical nutation) and will finally decay from the smaller QD, as schematically shown in Fig. 1(b). This suggests two different patterns of optical energy transfer, which appear depending on the occupation of the destination quantum dots. Another mechanism for realizing two different states is to induce resonance or nonresonance

between QD_S and QD_{L_1} due to many-body effects; details of this are discussed in Ref. 13.

B. Architecture for solving a constraint satisfaction problem: State-dependent energy transfer

To solve a constraint satisfaction problem (CSP) by using the optical energy transfer introduced in Sec. II A, we design an architecture where a smaller QD is surrounded by multiple larger QDs. In this paper, we assume four larger QDs, labeled QD_{L_1}, QD_{L_2}, QD_{L_3}, and QD_{L_4} as indicated in Fig. 2(a). Figure 2(c) shows representative parametrizations associated with the system. The (1,0) level in QD_S is denoted by S, and the (1,1) level in QD_{L_i} is denoted by $L_i^{(U)}$. These levels are resonant with each other and are connected by interdot interactions denoted by U_{SL_i} ($i = 1, \ldots, 4$). It should also be noted that

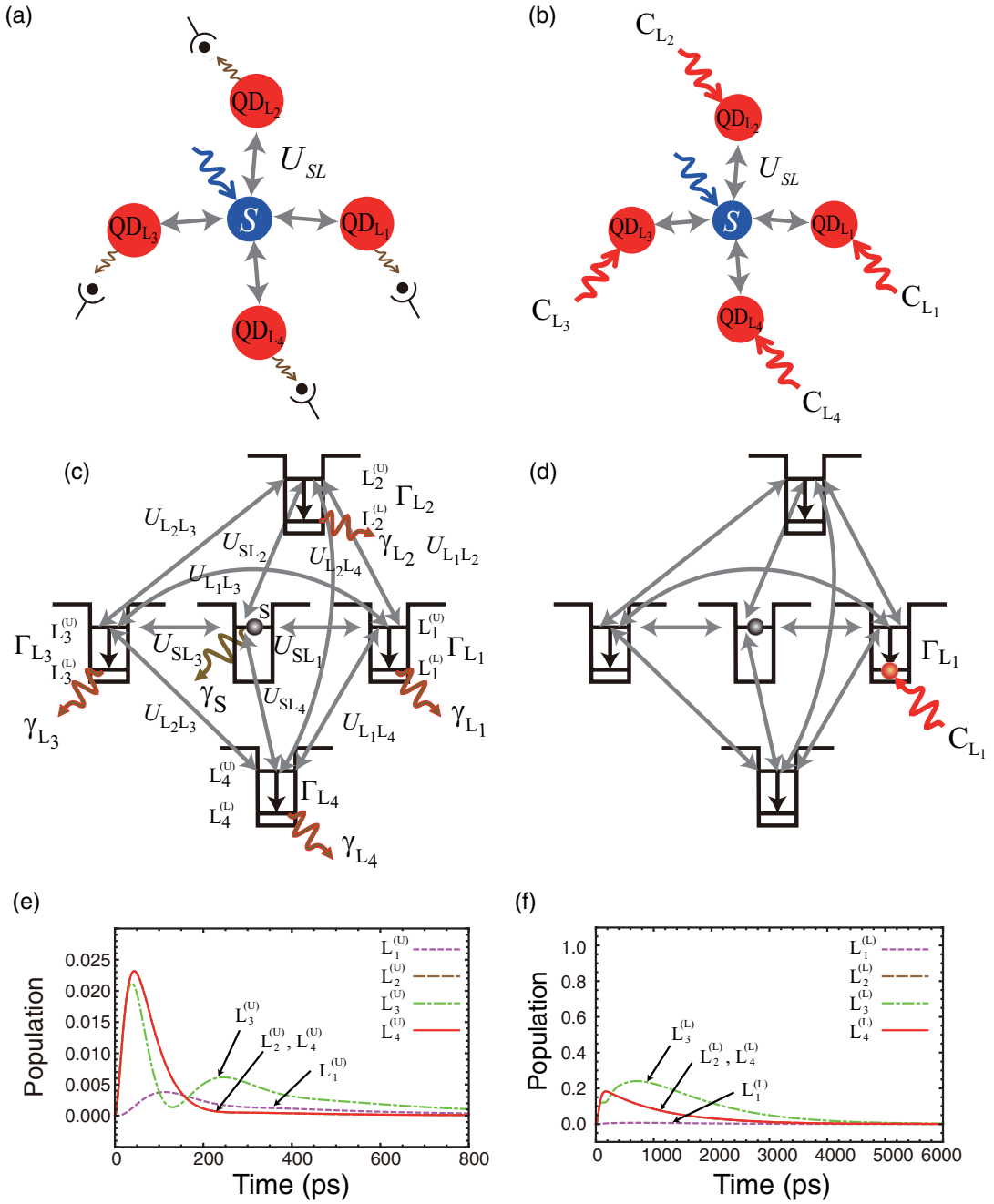

FIG. 2. (Color online) Architecture of the optical-energy-transfer–based satisfiability solver studied in this paper and energy diagram of a system composed of a smaller quantum dot and four larger quantum dots. (a) Radiation from the larger quantum dots is detected. (b) Control light for inducing state filling in the larger quantum dots. (c) Energy diagram and parametrization of the system. (d) A schematic diagram showing state filling induced at the lower energy level in QD_{L_1}. (e), (f) The effect of state filling induced in the lower energy level in QD_{L_1}. (e) Population evolutions for the upper energy levels in QD_{L_i} ($i = 1, \ldots, 4$) with two initial excitons: one exciton sits in S and the other sits in the lower energy level in QD_{L_1}. (f) Population evolutions for the lower energy levels in QD_{L_i} ($i = 1, \ldots, 4$) with one initial exciton in S while inducing a 100-times increase in the sublevel relaxation lifetime $\Gamma_{L_1}^{-1}$.

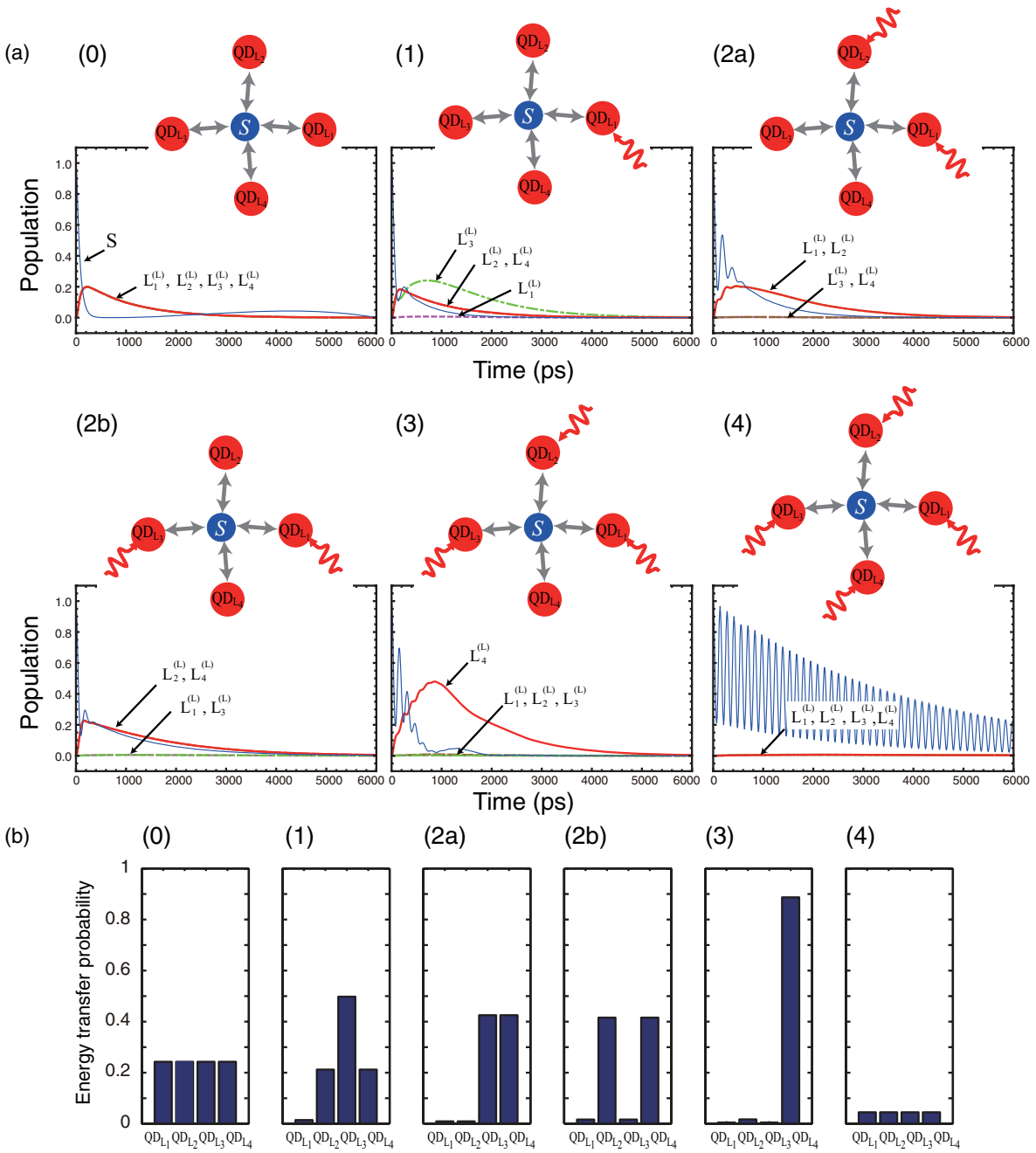

FIG. 3. (Color online) (a) Population evolutions for the lower energy levels in QD_{L_i} ($i = 1, \ldots, 4$) depending on the state filling induced at the larger dots. (b) Estimated energy transfer probabilities calculated as time integrals of the populations shown in (a).

optical near-field interactions between the (1,1) levels in QD_{L_i} and QD_{L_j} ($i \neq j$) are indicated by $U_{L_iL_j}$ in Fig. 3(c), which will be described in detail later below. Note that the interactions $U_{L_iL_j}$ are not shown in Figs. 2(a) and 2(b), nor are other illustrations regarding the architecture of the QD system in this paper, in order to avoid too much complexity in the figures. The lower level in QD_{L_i}, namely, the (1,0) level, is denoted by $L_i^{(L)}$, which could be filled via the sublevel relaxation from $L_i^{(U)}$ ($i = 1, \ldots, 4$), denoted by Γ_{L_i}. The radiations from the S and L_i levels are, respectively, represented by the relaxation constants γ_S and γ_{L_i} ($i = 1, \ldots, 4$). In the following discussion, we call the inverse of the relaxation constant the radiation lifetime. We also assume that the photons radiated from the lower levels of QD_{L_i} can be separately captured by photodetectors, as schematically shown in Fig. 2(a). In addition, as introduced in Sec. I, we assume control light, denoted by C_{L_i} in Fig. 2(b), so as to induce the state-filling effect at $L_i^{(L)}$. Summing up, Figs. 2(a) and 2(b) schematically represent the architecture of the system studied in this paper for solving a CSP. In this section, we characterize the basic behavior of optical energy transfer in the system shown in Figs. 2(a) and 2(b).

First, we suppose that the system initially has one exciton in S. From the initial state, through the interdot interactions U_{SL_i}, the exciton in S could be transferred to $L_i^{(U)}$ ($i = 1, \ldots, 4$).

Also, interactions exist between $L_i^{(U)}$, which are represented by $U_{L_iL_j}$. Accordingly, we can derive quantum master equations in the density matrix formalism.[23,25] The interaction Hamiltonian is given by

$$H_{\rm int} = \begin{pmatrix} 0 & U_{SL_1} & U_{SL_2} & U_{SL_3} & U_{SL_4} \\ U_{SL_1} & 0 & U_{L_1L_2} & U_{L_1L_3} & U_{L_1L_4} \\ U_{SL_2} & U_{L_1L_2} & 0 & U_{L_2L_3} & U_{L_2L_4} \\ U_{SL_3} & U_{L_1L_3} & U_{L_2L_3} & 0 & U_{L_3L_4} \\ U_{SL_4} & U_{L_1L_4} & U_{L_2L_4} & U_{L_3L_4} & 0 \end{pmatrix}. \quad (3)$$

The interdot near-field interactions are given by a Yukawa-type potential

$$U = \frac{A\exp(-\mu r)}{r}, \quad (4)$$

where r denotes the distance between the QDs, and A and μ are constants.[9,23]

The relaxation regarding these five states is described by

$$N_\Gamma = \begin{pmatrix} \frac{\gamma_S}{2} & 0 & 0 & 0 & 0 \\ 0 & \frac{\Gamma_{L_1}}{2} & 0 & 0 & 0 \\ 0 & 0 & \frac{\Gamma_{L_2}}{2} & 0 & 0 \\ 0 & 0 & 0 & \frac{\Gamma_{L_3}}{2} & 0 \\ 0 & 0 & 0 & 0 & \frac{\Gamma_{L_4}}{2} \end{pmatrix}. \quad (5)$$

The Liouville equation for the system is then

$$\frac{d\rho(t)}{dt} = -\frac{i}{\hbar}[H_{\rm int},\rho(t)] - N_\Gamma\rho(t) - \rho(t)N_\Gamma, \quad (6)$$

where $\rho(t)$ is the density matrix with respect to the five energy levels and $\hbar$ is Planck's constant divided by 2π. Similarly, we can derive differential equations with respect to the lower level of the larger dot $L_i^{(L)}$, which is populated by the relaxations from the upper energy levels with constants Γ_{L_i}, which radiatively decay with relaxation constants γ_{L_i}. In the numerical calculation, we assume $U_{SL_i}^{-1} = 100$ ps, $\Gamma_i^{-1} = 10$ ps, $\gamma_{L_i}^{-1} = 1$ ns, and $\gamma_S^{-1} = (R_L/R_S)^3 \times \gamma_{L_i}^{-1} \approx 2.92$ ns as a typical parameter set. For instance, in the experimental demonstrations based on a CdSe/ZnS core-shell QD shown in Ref. 26, the radiation lifetime of a CdSe/ZnS quantum dot with a diameter of 2.8 nm (larger QD) was measured to be 2.1 ns, which is close to the radiation lifetimes in the above parameter set. Also, the interaction time between smaller and larger quantum dots via optical near fields was estimated to be 135 ps in Ref. 26, which is also close to the above interdot interaction time.

The interactions between larger QDs, $U_{L_iL_j}$, could be obtained by referring to the geometry of the system, which is schematically shown in Figs. 2(a) and 2(b), and the Yukawa-type potential given by Eq. (4). For simplicity, we assume that these interaction times are the same as those between smaller and larger QDs, namely, $U_{L_1L_2}^{-1} = U_{L_2L_3}^{-1} = U_{L_3L_4}^{-1} = U_{L_1L_4}^{-1} = 100$ ps. On the other hand, the interactions between nonadjacent QDs, for example, the interaction between QD_{L_1} and QD_{L_3}, are considered to be weaker with regard to the geometry and the distance dependence given by Eq. (4). In this study, we assume that $U_{L_1L_3}^{-1} = U_{L_2L_4}^{-1} = 1000$ ps. Based on the above modeling and parametrizations, the calculated populations are represented in Fig. 3(a,0), where short-dashed (magenta), long-dashed (brown), dashed-dotted (green), and solid (red) curves, respectively, correspond to populations involving $L_1^{(L)}$, $L_2^{(L)}$, $L_3^{(L)}$, and $L_4^{(L)}$, which are relevant to the radiation from the larger QDs. The population with respect to S is also indicated by a thin solid curve (blue) in Fig. 3(a,0). Since the interdot optical near-field interactions between QD_S and QD_{L_i} are uniform, and the relaxation constants are also uniform for QD_{L_i}, the population evolutions exhibit the same patterns for QD_{L_i} ($i = 1,\ldots,4$), as shown in Fig. 3(a,0).

Second, we consider situations where one or more of the larger QDs are subjected to state filling by the control light C_{L_i} ($i = 1,\ldots,4$). Suppose, for example, that the control light C_{L_1} induces state filling at the energy level $L_1^{(L)}$, as schematically shown in Fig. 2(d). In order to take account of such state filling, we calculate the population evolutions with an initial state in which one exciton sits at S and another one is located at $L_1^{(L)}$. Based on a similar formalism to that described in Eqs. (3)–(6), we derive master equations for the two-exciton system, and combine them with those for the one-exciton system.[21] In order to characterize the differences of excitation transfer from QD_S to QD_{L_i} ($i = 1,\ldots,4$), we evaluate the populations for the upper energy levels in QD_{L_i}, that is $L_1^{(U)}$ ($i = 1,\ldots,4$). As shown in the solid curves in Fig. 2(e), the populations for $L_2^{(U)}$, $L_3^{(U)}$, and $L_4^{(U)}$ mostly exhibit larger values compared with that for $L_1^{(U)}$, which is shown by the dashed curve. This is a clear indication that optical energy is more likely to be transferred to QD_{L_2}, QD_{L_3}, and QD_{L_4} than to QD_{L_1}.

Another way of describing such an effect in the quantum master equations introduced above is by inducing a significant increase in the sublevel relaxation lifetime that corresponds to the QD_{L_i} subjected to state filling by the control light; more specifically, we assume that $\Gamma_{L_i}^{-1}$ increases by a factor of 1000 due to the control light C_{L_i}. Figure 2(f) characterizes the population evolutions associated with the energy levels in the system when the control light C_{L_1} is switched on. The population for $L_1^{(L)}$, shown by the dashed curve, stays at a lower level, whereas the populations for $L_2^{(L)}$, $L_3^{(L)}$, and $L_4^{(L)}$ increase. That is, Fig. 2(f) also shows that optical energy is more likely be transferred to QD_{L_2}, QD_{L_3}, and QD_{L_4} than to QD_{L_1}, which is consistent with the tendency shown in Fig. 2(e).

Looking at Figs. 2(e) and 2(f) in more detail, the populations for $L_2^{(U)}$ and $L_4^{(U)}$ exhibit different evolutions compared with that of $L_3^{(U)}$; this is because QD_{L_3} is located at the opposite side of QD_{L_1} where the control light is induced. Furthermore, the populations for $L_2^{(U)}$ and $L_4^{(U)}$ initially exhibit larger values compared with that for $L_3^{(U)}$; such behavior is also consistent in Figs. 2(e) and 2(f). Therefore, in the rest of this paper, we take the approach of inducing increases in $\Gamma_{L_i}^{-1}$ by using the control light C_{L_i}.

Figure 3(a) summarizes the population evolutions with respect to different numbers of control light beams. Figure 3(a,1) is the same as Fig. 2(f), as already explained, corresponding to the situation where $L_1^{(L)}$ is subjected to state filling. Figures 3(a,2a) and 3(a,2b) show the populations when two levels among $L_i^{(L)}$ are subjected to state filling. The relative position of the two QDs subjected to control light are different between Figs. 3(a,2a) and 3(a,2b). Figure 3(a,3) shows the

populations when three levels among $L_i^{(L)}$ are subjected to state filling. The energy transfer preferentially flows into the larger dots that are not subjected to state filling with the control light. When all of the larger dots are subjected to state filling, the exciton sitting in the level S initially goes back and forth among the levels S and $L_i^{(U)}$ and decays from the level S, as observed by the solid thin curve in Fig. 3(a,4). The differences in the population evolutions shown in Fig. 3(a) depending on the control light C_{L_i} suggest differences in energy transfer probabilities from the smaller source dot to the larger destination dots. Taking account of such differences, we assume that the energy transfer probability to QD_{L_i} is correlated with the integrals of the populations for $L_i^{(L)}$, as summarized in Fig. 3(b). More specifically, the transition probabilities shown in Fig. 3(b) are the numerical integrations of the populations between 0 and 20 ns divided by a factor of 1000. Note that such population integrals are indeed figures-of-merit (FoM) indicating the trend of optical energy transfer from the smaller quantum dot to the four larger dots. That is, they do *not* satisfy the law of conservation of probability, namely, the sum of the transition probabilities to QD_{L_i} $(i = 1, \ldots, 4)$ is not unity. Instead, we see that the energy transfer to QD_{L_i} occurs if a uniformly generated random number between 0 and 1 is less than the transition probability to QD_{L_i} shown in Fig. 3(b); for example, in the case of Fig. 3(b,3), the energy transfer to QD_{L_4} is induced with high likelihood, whereas the transfers to QD_{L_1}, QD_{L_2}, and QD_{L_3} are induced with lower probability.

The idea for problem solving is to control the optical energy transfer by controlling the destination quantum dot with control light in an adequate feedback mechanism. We assume that a photon radiated, or observed, from the energy level $L_i^{(L)}$ is equivalent to a binary value x_i having a logical level 1, whereas the absence of an observed photon means $x_i = 0$.

To end this section, we make one remark about "nonlocal" properties of the system. The interaction Hamiltonian includes distant interactions $U_{L_1L_3}$ and $U_{L_2L_4}$, not just interactions between adjacent dots. In that sense, a "nonlocal" nature has been treated in this study. Furthermore, we consider that the state-filling-dependent population differences summarized in Fig. 3 also manifest a nonlocal property. The initial exciton sitting in QD_S can be transferred to the upper energy levels of the larger QD via optical near-field interactions. Seemingly, the exciton immediately senses the vacancy in the destination, or larger, QD, and exhibits different energy transfer patterns. For instance, in the case of Fig. 3(a,3), the probability of energy transfer to QD_{L_4} is significantly higher than in the other cases. This can be viewed as a "nonlocal" property in the sense that it is a consequence of the character of the system as a whole.

III. APPLICATION TO SOLVING A CONSTRAINT SATISFACTION PROBLEM

A. Problem formation

We consider the following constraint satisfaction problem as an example regarding an array of N binary-valued variables $x_i \in \{0,1\}\,(i = 1, \ldots, N)$. The constraint is that $x_i =$ NOR(x_{i-1}, x_{i+1}) should be satisfied for all i. That is, variable x_i should be consistent with a logical NOR operation of the two neighbors. For $i = 1$ and N, the constraints are respectively given by $x_1 =$ NOR(x_N, x_2) and $x_N =$ NOR(x_{N-1}, x_1). We call this problem the "NOR problem" hereafter in this paper. Taking account of the nature of an individual NOR operation, one important inherent character is that, if $x_i = 1$ then its two neighbors should be both zero $(x_{i-1} = x_{i+1} = 0)$. Recall that a photon radiated, or observed, from the energy level $L_i^{(L)}$ corresponds to a binary value $x_i = 1$, whereas the absence of an observed photon means $x_i = 0$. Therefore, $x_i = 1$ should mean that the optical energy transfer to both $L_{i-1}^{(L)}$ and $L_{i+1}^{(L)}$ is prohibited so that $x_{i-1} = x_{i+1} = 0$ is satisfied. Therefore, the feedback or control mechanism is as follows: *Control mechanism*. If $x_i = 1$ at cycle t, then the control light beams C_{i-1} and C_{i+1} are turned on at cycle $t = t + 1$. An example scheme is illustrated in Fig. 4.

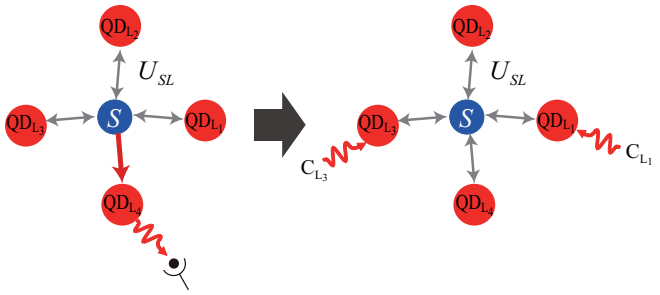

FIG. 4. (Color online) A schematic representation of the feedback mechanism. When the radiation from QD_{L_4} is detected in cycle t, control light beams C_{L_1} and C_{L_3}, which are in channels adjacent to QD_{L_4}, are switched on.

In the case of $N = 4$, variables satisfying the constraints do exist, and they are given by $\{x_1, x_2, x_3, x_4\} = \{0,1,0,1\}$ and $\{1,0,1,0\}$, which we call "correct solutions." There are a few remarks that should be made regarding the NOR problem. One is about the potential deadlock, analogous to Dijkstra's "dining philosophers problem," as already argued by Aono *et al.* in Ref. 4. Starting with an initial state $x_i = 0$ for all i, and assuming a situation where optical energy is transferred to all larger QDs, we observe photon radiation from all energy levels $L_i^{(L)}$ $(i = 1, \ldots, N)$, namely, $x_i = 1$ for all i. Then, based on the feedback mechanism shown above, all control light beams are turned on. If such a feedback mechanism perfectly inhibits the optical energy transfer from the smaller QD to the larger ones at the next step $t + 1$, the variables then go to $x_i = 0$ for all i. This leads to all control light beams being turned off at $t + 2$. In this manner, all variables constantly repeat periodic switching between $x_i = 0$ and 1 in a synchronized manner. Consequently, the system can never reach the correct solutions. However, as indicated in Fig. 3(b), the probability of optical energy transfer to larger dots is in fact not zero even when all larger QDs are illuminated by control light, as shown in Fig. 3(b,4). Also, even for a nonilluminated destination QD, the energy transfer probability may not be exactly unity. Such a stochastic behavior of the optical energy transfer is a key role in solving the NOR problem. This nature is similar to the demonstrations in the amoeba-based computer,[4] where fluctuations of chaotic oscillatory behavior

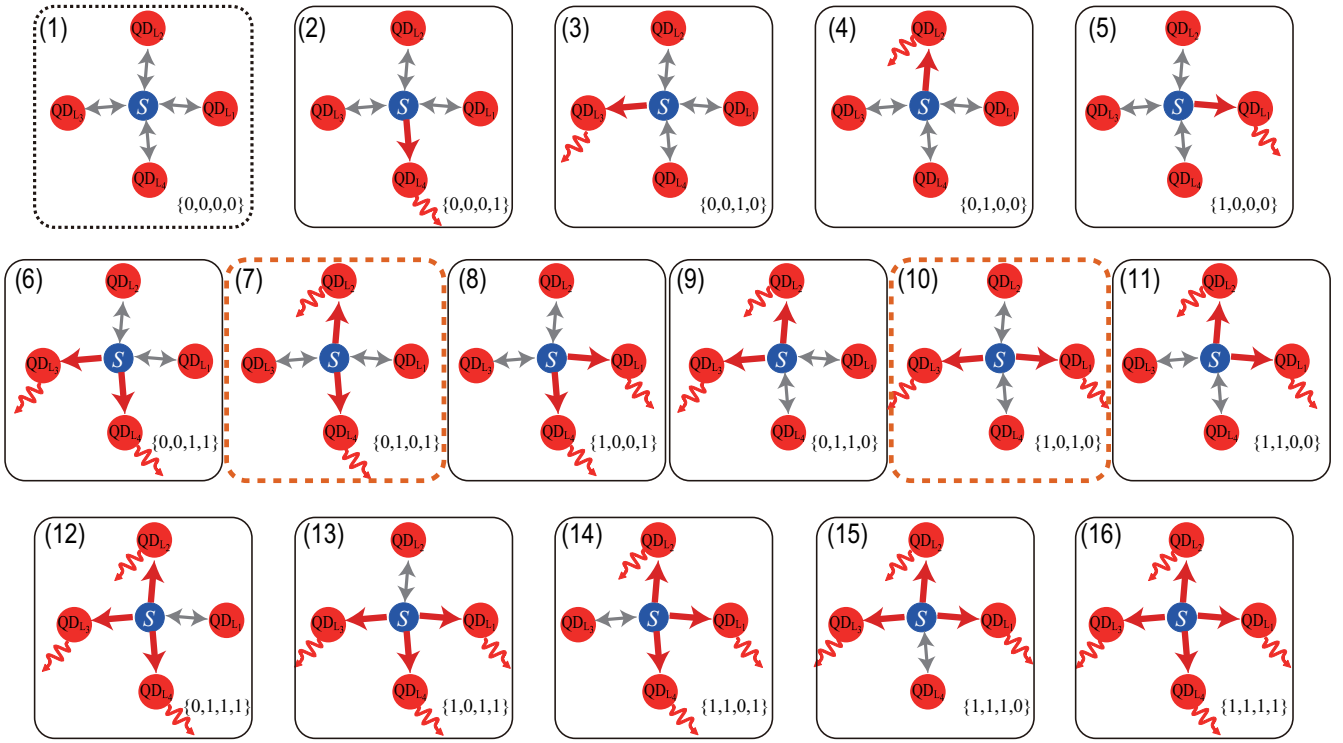

FIG. 5. (Color online) Schematic representation of all possible states of the system. States (7) and (10) correspond to the correct solutions.

involving spontaneous symmetry breaking in the amoeboid organism guarantees such a critical property. In fact, Aono *et al*. experimentally demonstrated solving the NOR problem when $N = 8$ using amoeba and the feedback mechanism shown above.[4]

B. Demonstration

In the case of $N = 4$, there are in total $2^4 = 16$ optical energy transfer patterns from the smaller dot to the larger ones, as schematically summarized in Fig. 5. The numbers shown in the lower-right corner of each inset indicate the corresponding variables $\{x_1,x_2,x_3,x_4\}$. The correct solutions correspond to states (7) and (10) in Fig. 5, marked by dashed boxes. The operating dynamics cause one pattern to change to another one in every iteration cycle. Thanks to the stochastic nature discussed in Secs. II B and III A, each trial could exhibit a different evolution of the energy transfer patterns. In particular, the transition probability, shown in Fig. 3(b), affects the behavior of the transitions. Therefore, we introduce a gain factor (G) to be multiplied by the energy transfer probability summarized in Fig. 3(b).

Figure 6 summarizes the incidences of states for 1000 trials evaluated at $t = 1$, 2, 3, 50, and 100 when $G = 2.5$. The initial state is $\{x_1,x_2,x_3,x_4\} = \{0,0,0,0\}$, meaning that there is no energy transfer to larger dots [state (1) in Fig. 5]. The incidences of states (7) and (10), which are the correct solutions, grow as the iteration cycle increases. The detailed

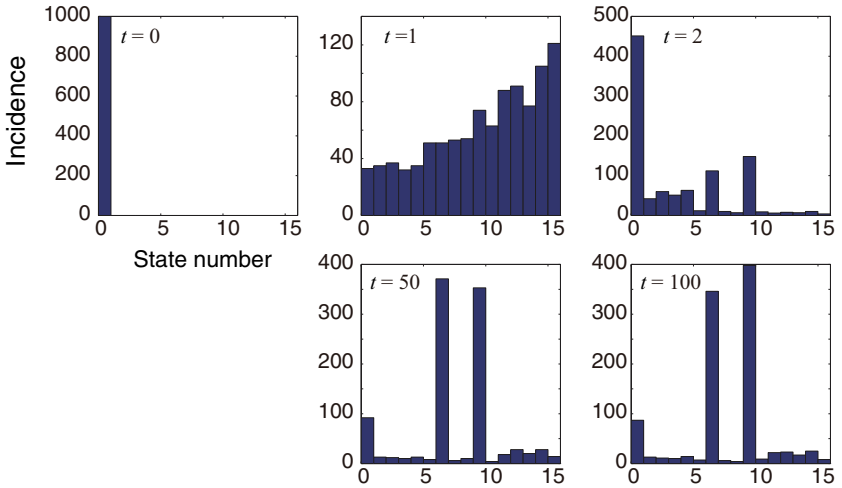

FIG. 6. (Color online) The evolution of incidence patterns of the states among 1000 trials when the gain factor is 2.5. The incidences corresponding to the correct solutions increase as the iteration cycle increases.

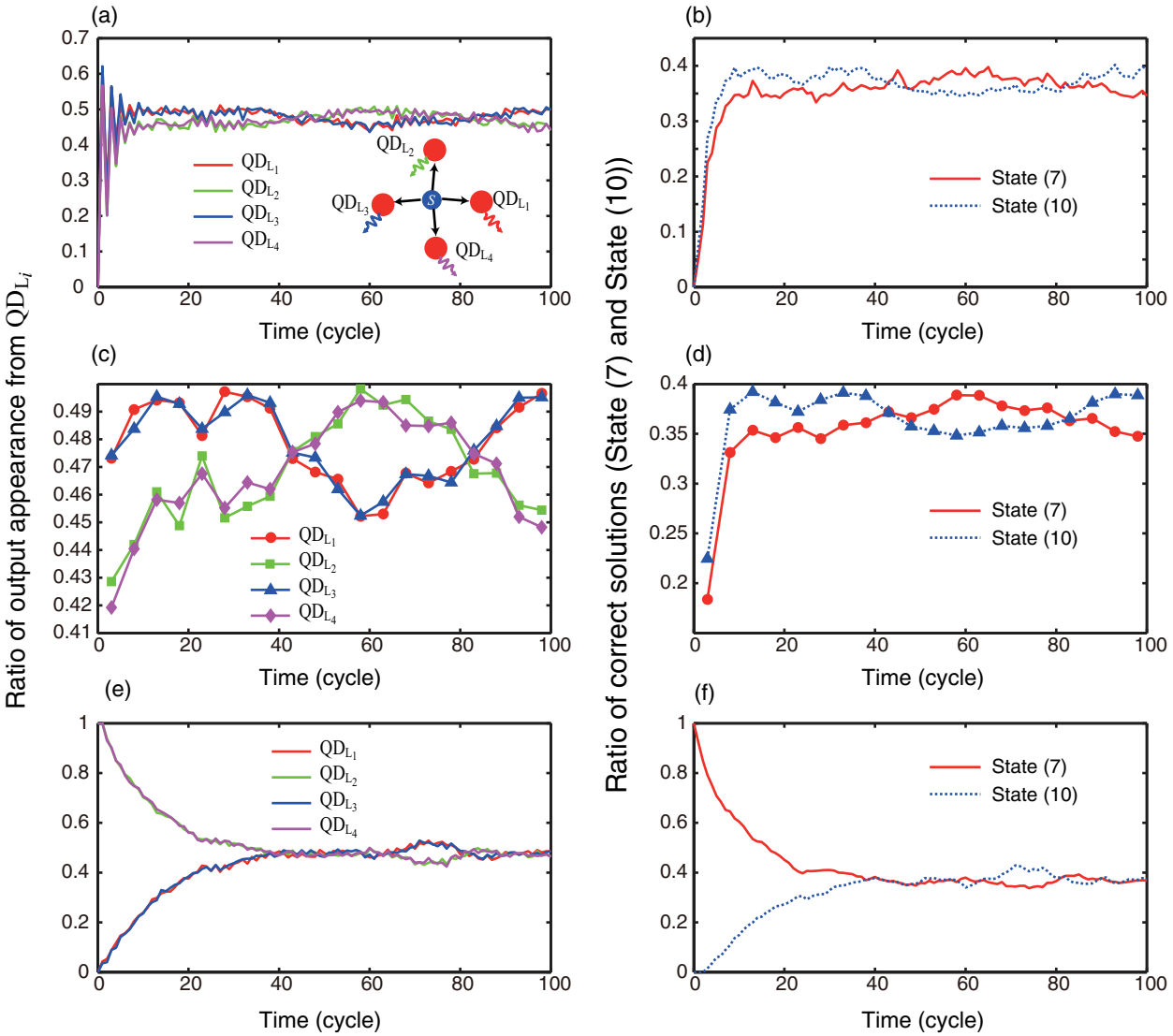

FIG. 7. (Color online) (a) The evolution of the ratio of the output appearance from QD_{L_i}, or $x_i = 1$, and (b) the ratio of the state corresponding to the correct solutions with the initial state (1) in Fig. 5. (c), (d) Time-averaged traces of (b) and (c), respectively. (e) The evolution of the ratio of the output appearance from QD_{L_i}, or $x_i = 1$, and (f) the ratio of the state corresponding to correct solutions with the initial state of (7) in Fig. 5.

behavior of the system is characterized in Figs. 7(a) to 7(d). The curves in Fig. 7(a) represent the evolution of the output appearance from QD_{L_i}, namely, the ratio of the incidence when $x_i = 1$ among 1000 trials evaluated at each cycle. Similarly, the solid and dotted curves in Fig. 7(b) characterize the ratio of the appearance of states (7) and (10), respectively. When we closely examine the evolutions of x_i in Fig. 7(a), we can see that the pair x_1 and x_3 exhibit similar behavior, as do the pair x_2 and x_4. Also, the former pair exhibits larger values when the latter pair shows smaller values, and vice versa. This corresponds to the fact that correct solutions, that is, {0,1,0,1} [state (7)] and {1,0,1,0} [state (10)], are likely to be induced as the iteration cycle increases, as shown in Fig. 6.

Such a tendency is more clearly represented when we evaluate the time averages of the characteristics in Figs. 7(a) and 7(b). Figure 7(c) shows the evolution of the ratio of the incidences when $x_i = 1$, and Fig. 7(d) shows the ratios of states (7) and (10) averaged over every five cycles. We can clearly observe a similar tendency to the one described above. Also, we should emphasize that, thanks to the probabilistic nature of the system, the states of correct solutions appear in an interchangeable, or in an anticorrelated, manner. This is a clear indication of the fact that the probabilistic nature of the system autonomously seeks the solutions that satisfy the constraints of the NOR problem; the state-dependent probability of energy transfer plays a critical role in this. In other words, it should be emphasized that a nonlocal correlation is manifested in the evolution of x_i ($i = 1, \ldots, 4$); for instance, when the system is in state (7), i.e., {0,1,0,1}, the probabilities of energy transfer to QD_{L_1} and QD_{L_3} are equally comparably low (due to state filling), whereas those to QD_{L_2} and QD_{L_4} are equally comparably high, indicating that the probability of energy transfer to an individual QD_{L_i} has inherent spatial patterns or nonlocal correlations. At the same time, the energy transfer

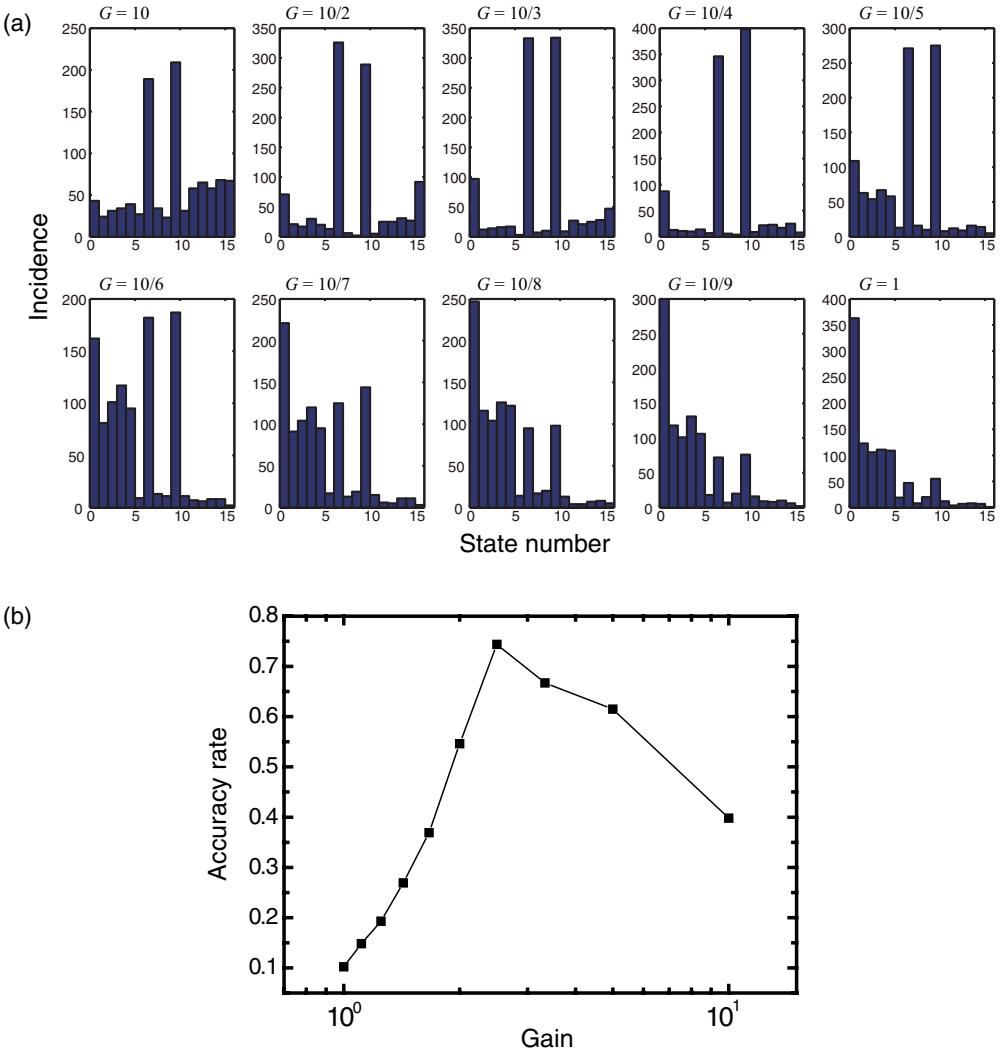

FIG. 8. (Color online) (a) The incidence patterns of the states for different gain factors at the cycle $t = 100$. (b) Calculated accuracy rate, or the ratio of the number of correct states among all trials. The accuracy rate is maximized when the gain factor is 2.5.

to each QD_{L_i} is indeed probabilistic; therefore, the energy transfer probability to, for instance, QD_{L_1} is not zero even in state (7), and thus, the state could transition from state (7) to state (10), and vice versa. In fact, starting with the initial condition of state (7), the ratio of the output appearance from QD_{L_1} and the ratio of the correct solutions evolve as shown in Figs. 7(e) and 7(f), where states (7) and (10) occur equally in the steady state around time cycles after 20.

Figure 8(a) summarizes the incidence patterns at $t = 100$ for 1000 trials as a function of the gain factor ranging from 1 to 10. As shown in the upper-left corner of Fig. 8(a), too high a gain always results in incorrect solutions; this is because energy transfers to larger dots are always induced even when state filling is induced. On the other hand, as shown in the lower-right corner of Fig. 8(a), too low a gain also results in a high incidence of incorrect solutions, indicating that the energy transfer is too strictly inhibited by the control light. Figure 8(c) evaluates the accuracy rate, which is the number of correct solutions among 1000 different trials at $t = 100$, as a function of the gain factor. We can see that a gain of 2.5 provides the highest accuracy rate.

Finally, we make two remarks relevant to this study. The first remark is about the relevance to a satisfiability (SAT) problem. In the case of $N = 4$, solving the NOR problem demonstrated above is equivalent to solving the following satisfiability problem instance given in a conjunctive normal form:

$$\begin{aligned} f(x_1,x_2,x_3,x_4) = {} & (\neg x_1 \vee \neg x_2) \wedge (\neg x_1 \vee \neg x_4) \\ & \times \wedge (\neg x_2 \vee \neg x_3) \wedge (\neg x_3 \vee \neg x_4) \\ & \times \wedge (x_1 \vee x_2 \vee x_3) \wedge (x_1 \vee x_2 \vee x_4) \\ & \times \wedge (x_1 \vee x_3 \vee x_4) \wedge (x_2 \vee x_3 \vee x_4). \end{aligned} \quad (7)$$

Since the maximum number of literals in clauses in Eq. (7) is three, this is an instance of a so-called 3SAT problem.[27] We presume that such a SAT problem could be dealt with by variants of our optical-near-field–mediated systems developed in the future.[28] SAT is an important nondeterministic polynomial-time complete (NP-complete) problem, indicating that no fast algorithm has been found yet.[27] We consider that nanophotonic principles could potentially provide a new way to solve such computationally demanding problems.

The second remark is about implementation of optical energy transfer for such stochastic computing applications. As mentioned in the Introduction, the latest notable features are the rapid advancements in nanomaterials for optical energy transfer.[10–16] Among various technologies, for example, Akahane *et al*. successfully demonstrated energy transfer in multistacked InAs QDs,[29] where layer-by-layer QD size control has been accomplished.[13] Adequate QD size control also allows optical coupling between optical far fields and optically allowed energy levels in a quantum-dot mixture,[30] which could help to solve the interfacing issues of the system. Research in the field of nanodiamonds may also be of promise in implementing the architecture of this study;[17,18] near-field applications of nanodiamonds have already been demonstrated by Cuche *et al*. in Ref. 31.

IV. SUMMARY

In summary, we have demonstrated that energy transfer between quantum nanostructures based on optical near-field interactions occurring at scales far below the wavelength of light has the potential to solve a constraint satisfaction problem. The optical energy transfer from smaller quantum dots to larger ones, which is a quantum stochastic process, depends on the existence of resonant energy levels between the quantum dots or a state-filling effect occurring at the destination quantum dots. We exploit these unique spatiotemporal mechanisms in optical energy transfer to solve a constraint satisfaction problem, and numerically demonstrated that the NOR problem is successfully solved. As indicated in the Introduction, the concept and the principles demonstrated in this paper are based on both coherent and dissipative processes on the nanoscale, which is not the case with conventional optical, electrical, and quantum computing paradigms. The inherently nonlocal nature is also a unique attribute provided by the optical-near-field–mediated optical energy transfer. This paper paves the way for applying nanometer-scale optical near-field processes to solving computationally demanding applications and suggests a new computing paradigm.

ACKNOWLEDGMENT

This work was supported in part by the Strategic Information and Communications R&D Promotion Programme (SCOPE) of the Ministry of Internal Affairs and Communications, and Grants-in-Aid for Scientific Research from the Japan Society for the Promotion of Science.

*naruse@nict.go.jp

[1] *International Technology Roadmap for Semiconductors*, 2009 Edition, Emerging Research Devices.
[2] *Brain-like Computing and Intelligent Information Systems,* edited by S. Amari and N. Kasabov (Springer, Singapore, 1998).
[3] L. B. Kish, Phys. Lett. A **373**, 911 (2009).
[4] M. Aono, M. Hara, and K. Aihara, Commun. ACM **50**, 69 (2007).
[5] T. Nakagaki, H. Yamada, and A. Toth, Nature (London) **407**, 470 (2000).
[6] M. Aono, L. Zhu, and M. Hara, Int. J. Unconventional Comput. **7**, 463 (2011).
[7] K. Leibnitz and M. Murata, IEEE Network, Special Issue on Biologically Inspired Networking **24**, 14 (2010).
[8] M. Naruse, T. Miyazaki, T. Kawazoe, S. Sangu, K. Kobayashi, F. Kubota, and M. Ohtsu, IEICE Trans. Electron. **E88-C**, 1817 (2005).
[9] M. Ohtsu, T. Kawazoe, T. Yatsui, and M. Naruse, IEEE J. Sel. Top. Quantum Electron. **14**, 1404 (2008).
[10] T. Kawazoe, K. Kobayashi, K. Akahane, M. Naruse, N. Yamamoto, and M. Ohtsu, Appl. Phys. B **84**, 243 (2006).
[11] T. Yatsui, S. Sangu, T. Kawazoe, M. Ohtsu, S. J. An, J. Yoo, and G.-C. Yi, Appl. Phys. Lett. **90**, 223110 (2007).
[12] W. Nomura, T. Yatsui, T. Kawazoe, M. Naruse, and M. Ohtsu, Appl. Phys. B **100**, 181 (2010).
[13] T. Kawazoe, M. Ohtsu, S. Aso, Y. Sawado, Y. Hosoda, K. Yoshizawa, K. Akahane, N. Yamamoto, and M. Naruse, Appl. Phys. B **103**, 537 (2011).
[14] M. Naruse, H. Hori, K. Kobayashi, P. Holmström, L. Thylén, and M. Ohtsu, Opt. Express **18**, A544 (2010).
[15] K. Akahane, N. Yamamoto, and M. Tsuchiya, Appl. Phys. Lett. **93**, 041121 (2008).
[16] C. Pistol, C. Dwyer, and A. R. Lebeck, IEEE Micro. **28**, 7 (2008).
[17] Y. Dumeige, F. Treussart, R. Alleaume, T. Gacoin, J.-F. Roch, and P. Grangier, J. Lumin. **109**, 61 (2004).
[18] N. Mohan, Y.-K. Tzeng, L. Yang, Y.-Y. Chen, Y. Y. Hui, C.-Y. Fang, and H.-C. Chang, Adv. Mater. **22**, 843 (2010).
[19] H. J. Caulfield and S. Dolev, Nat. Photonics **4**, 261 (2010).
[20] D. P. DiVincenzo, Science **270**, 255 (1995).
[21] M. Naruse, T. Kawazoe, R. Ohta, W. Nomura, and M. Ohtsu, Phys. Rev. B **80**, 125325 (2009).
[22] H. Haug and S. W. Koch, *Quantum Theory of the Optical and Electronic Properties of Semiconductors* (World Scientific, Singapore, 2004).
[23] M. Ohtsu, K. Kobayashi, T. Kawazoe, T. Yatsui, and M. Naruse, *Principles of Nanophotonics* (Taylor and Francis, Boca Raton, 2008).
[24] T. Itoh, M. Furumiya, T. Ikehara, and C. Gourdon, Solid State Commun. **73**, 271 (1990).
[25] H. J. Carmichael, *Statistical Methods in Quantum Optics 1* (Springer, Berlin, 1999).
[26] W. Nomura, T. Yatsui, T. Kawazoe, and M. Ohtsu, J. Nanophotonics **1**, 011591 (2007).
[27] B. Korte and J. Vygen, *Combinatorial Optimization: Theory and Algorithms* (Springer, Berlin, 2012).
[28] M. Aono, S.-J. Kim, L. Zhu, M. Naruse, M. Ohtsu, H. Hori, and M. Hara, The 2012 International Symposium on Nonlinear Theory and its Applications (NOLTA 2012) (to be published).
[29] K. Akahane, N. Yamamoto, M. Naruse, T. Kawazoe, T. Yatsui, and M. Ohtsu, Jpn. J. Appl. Phys. **50**, 04DH05 (2011).
[30] M. Naruse, T. Kawazoe, S. Sangu, K. Kobayashi, and M. Ohtsu, Opt. Express **14**, 306 (2006).
[31] A. Cuche, A. Drezet, Y. Sonnefraud, O. Faklaris, F. Treussart, J.-F. Roch, and S. Huant, Opt. Express **17**, 19969 (2009).